



## Research Article

# Numerical simulation of flow and dam body sediment over a movable bed due to an earthfill dam break

Gokmen TAYFUR<sup>1\*</sup>, Alibek ISSAKHOV<sup>2</sup>, Yeldos ZHANDAULET<sup>2</sup>

<sup>1</sup>Department Civil Engineering, Izmir Institute of Technology, Izmir, Türkiye

<sup>2</sup>Al-Farabi Kazakh National University, Almaty, Kazakhstan

## ARTICLE INFO

### Article history

Received: 22 January 2021

Accepted: 26 April October 2021

### Keywords:

Earthfill-dam; Dam-break;  
Sediment; RANS; k- $\omega$ ; PISO;  
Model; Simulation

## ABSTRACT

This paper presents the numerical simulations of flow and dam body sediment transport over a movable bed due to an earthfill dam break. The RANS equations, together with the k- $\omega$  SST turbulent model, are employed. The phase characteristic parameter is used as the phases of air, water, sediment, and bulk of dam body. The system of equations is solved numerically using the PISO algorithm. The numerical model is first verified using the dam break experimental data from the literature. The model successfully captures the temporal changes in the measured flow depths, pressures, wave fronts, and arrival times. The verified model is then applied to simulate the flow and sediment transport as a result of an artificial earthfill dam break having an obstacle at its downstream section. The simulations show that there is a noticeable decrease in the shock pressures at all points around the obstacle and there is an increase in the water levels. The bulk dam body sediment moves together with the water flow while spreading. It takes longer time for the sediment laden flow to reach the obstacle. The investigation of dam body formed by different soils shows that the soil type has minor effect while the transport of sediment can raise the water levels and change the morphology of the downstream section.

**Cite this article as:** Tayfur G, Issakhov A, Zhandulet Y. Numerical simulation of flow and dam body sediment over a movable bed due to an earthfill dam break. Sigma J Eng Nat Sci 2022;40(3):543–557.

## INTRODUCTION

Earthfill dams have been widely built all over the world due to mainly economical reasons. These dams however are prone to failures as a result of erratic seeping, piping, insufficient spillway capacity, overflows and extreme inflows.

The most recent examples are Patel Milmet Embankment Dam in Kenya failed on 9 May 2018 and Laos Embankment Dam in Vietnam failed on July 23, 2018 due to extreme inflows [1]. When such dams fail not only water but also

### \*Corresponding author.

\*E-mail address: gokmentayfur@iyte.edu.tr, alibek.issakhov@gmail.com, bashkantktl@gmail.com

This paper was recommended for publication in revised form by Regional Editor Abdelraheem Mahmoud Aly



dam body sediment transport occurs, resulting in an inundation of downstream area with muddy flow causing severe damage to human lives and livestock. For example, as a result of the failures of these two dams, about 190 people were buried under the mud ([https://en.wikipedia.org/wiki/Patel\\_Dam\\_failure](https://en.wikipedia.org/wiki/Patel_Dam_failure); [https://en.wikipedia.org/wiki/2018\\_Laos\\_dam\\_collapse](https://en.wikipedia.org/wiki/2018_Laos_dam_collapse)).

Dam failures are thus studied experimentally and numerically. Experimental and numerical studies are carried out in one-dimension [2]-[5], in two-dimensions [6]-[12] and in three dimensions [13]-[17]. In the experimental studies, the dam body is generally represented by a movable metal and thus the sediment transport part of the physical process is ignored [18]-[21]. Thus, the researchers, in their experimental and numerical studies, have mostly concentrated on the water flow part. However, as the recent dam failures show, when such dams fail, both water and sediment transport play crucial role. Therefore, there is a need to develop models considering both transport.

The main problems in the existing numerical methods in terms of a fluid-solid modelling can be many folds; (1) describing the interface position, (2) tracking the moving interfaces, (3) implementing the moving boundary conditions, (4) having the discontinues interfaces, (5) having the breaking waves, and (6) determining the dynamic pressure loads when exposed to several phases. Good interface capturing method in modeling the high density multiphase flows requires not only the sufficient numerical accuracy, but also the mass conservation. The particle methods, based on the Lagrangian framework for simulating the multiphase flows, contain the hydrodynamics of smoothed particles [22], the finite elements method (FEM) without a mesh [23] and the FEM of particles [24]. These methods have been extended by many researchers to model a wide class of problems associated with complex interactions between liquids and solids due to their high computational efficiency and simplicity [25]-[28]. However, these methods have some restrictions, such as the lack of instability and consistency in tension due to the distortion of the material region, which can lead to low accuracy and problems in satisfying the required convergence. Artificial viscosity is considered as an important problem in the SPH (Smoother Particle Hydrodynamics) applications [20], [29]. Furthermore, for the FEM of particles, the mesh size and the number of the particles are considered as significant parameters [30].

In the Eulerian approach, however, the level setting method [28] and many more advanced numerical methods are suggested for more accurate modeling of the multiphase flows [31]-[37]. The level setting methods are simple but less accurate, and thus the reinitialization methods are generally used to increase their accuracy. Alternatively, the Volume of Fluid (VOF) [38] methods, such as the simple linear interface calculation algorithm, the piecewise linear interface calculation algorithm, and the VOF least squares

reconstruction algorithm are well known for reasonably conserving the mass and they are often used by researchers to simulate the multiphase flows [39]-[43]. The VOF method has significantly increased the range of performance, accuracy and applicability. With the development of computer technology, the VOF has been applied to simulate many real large-scale engineering problems such as the dam break flows [5], [6], [17], [44], and [45].

Numerical models simulating the flows containing sediment in a flow field are also developed [46] and [47]. Bao et al. [47] carried out the numerical calculations, the geomorphological analysis, and the laboratory measurements to estimate the extent of potential debris flows. Marsooli and Wu [46] developed a three-dimensional (3D) numerical model for modeling flows during a dam break with sediment transport. The hydrodynamic part of the model is described by the three-dimensional Reynolds Averaged Navier-Stokes (RANS) equations. The non-cohesive sediment transport dynamics is described by three more partial differential equations (for suspended sediment concentration, sediment rate, and bed elevation). For the numerical solution, they employed the finite volume method with a compression boundary capture scheme. Although the model of Marsooli and Wu [46] is a comprehensive model, it requires heavy numerical computational burden due to solving five very highly nonlinear partial differential equations.

The objective of this study is to develop a more efficient and reliable numerical solver for modeling the process of water flow and sediment transport as a result of an earthfill dam break. It proposes to consider the sediment as a third phase, supplementing the phases of air and water. In this way, three partial differential equations would be numerically solved. The solution would then be much faster and more efficient during the modelling process.

The article is structured as having 6 sections: The introduction is given in Section 1. The governing equations are presented in Section 2 while the Numerical Algorithm is described in Section 3. Section 4 involves the validation of the numerical model with the idealized dam break flows over fixed and movable beds while Section 5 contains the application of the numerical model using the laboratory experiments of earthfill dam breaks over fixed and movable beds. The Conclusions are presented in Section 6.

## GOVERNING EQUATIONS

This study treated the dynamics of the process as having the four phases: water, air, sediment, and bulk dam. The RANS equations are employed for the incompressible fluid flow [17]:

$$\frac{\partial u_j}{\partial x_j} = 0 \quad (1)$$

$$\frac{\partial u_i}{\partial t} + \frac{\partial u_i u_j}{\partial x_j} = g - \frac{1}{\rho} \frac{\partial P}{\partial x_i} + \frac{1}{\rho} \frac{\partial}{\partial x_j} \left[ (\mu + \mu_t) \left( \frac{\partial u_i}{\partial x_j} + \frac{\partial u_j}{\partial x_i} \right) \right] \quad (2)$$

$$\frac{\partial \chi}{\partial t} + u_j \frac{\partial \chi}{\partial x_j} = 0 \quad (3)$$

where  $u$  is the flow velocity,  $g$  is the gravitational acceleration,  $P$  is the pressure,  $\rho$  is the fluid density,  $\mu$  is the dynamic viscosity,  $\mu_t$  is the eddy viscosity;  $\chi$  is the phase characteristic,  $\chi = \alpha_q \rho_q$  (where  $\rho_q$  is volume fraction of  $q^{\text{th}}$  phase (can be fluid, air or sediment) in the cell,  $\rho_q$  is the density of  $q^{\text{th}}$  phase),  $i$  and  $j$  stand for the  $x$ -,  $y$ -, and  $z$ -directions.

The phase characteristic ( $\chi$ ) is the fundamental parameter in the VOF formulation when solving the multiphase fluid flow transport. In each control volume, the volume fractions of all phases sum to unity. The fields for all variables and properties are shared by the phases and represented by the volume-averaged values, as long as the volume fraction of each phase is known at each location. Thus, the variables and properties in any given cell are either purely representative of one of the phases, or representative of a combination of the phases, depending upon the volume fraction values. In other words, if  $q^{\text{th}}$  fluid-phase volume fraction in the cell is denoted as  $\alpha_q$ , then three conditions are possible:  $\alpha_q = 0$ ; the cell is empty of  $q^{\text{th}}$  fluid,  $\alpha_q = 1$ ; the cell is full of  $q^{\text{th}}$  fluid;  $0 < \alpha_q < 1$ , the cell contains the interface between  $q^{\text{th}}$  fluid and one or more other phases. Based on the local value of  $\alpha_q$  the appropriate properties and variables are assigned to each control volume within the domain. The volume fraction equation is not solved for the primary phase; the primary-phase volume fraction is computed based on the constraint of  $\sum_{q=1}^n \alpha_q = 1$ . In this study, four phases ( $n = 4$ )

as air ( $q = 1$ ), water ( $q = 2$ ), sediment ( $q = 3$ ) and bulk dam ( $q = 4$ ) are used in the modelling procedure for the fluid-sediment transport as a result of earthfill dam break.

The tensor stress in the incompressible Newtonian fluids is proportional to the strain rate tensor  $\vec{D}$  as [17] and [48]:

$$\vec{\tau} = \mu \vec{D} \quad (4)$$

$$\vec{D} = \left( \frac{\partial u_j}{\partial x_i} + \frac{\partial u_i}{\partial x_j} \right) \quad (5)$$

The tensor stress for the non-Newtonian fluids is determined as:

$$\vec{\tau} = \eta(\vec{D}) \vec{D} \quad (6)$$

where  $\eta$  is a three invariants function of the strain rate tensor  $\vec{D}$  [44].

To close the RANS equations, the  $k$ - $\omega$  SST (shear stress transport) turbulent model with two additional equations for the two variables  $k$  and  $\omega$  is employed. Issakhov et al. [44] employed several methods to close the RANS equations and concluded that the  $k$ - $\omega$  was the better one, especially with respect to the CPU time. For the Newtonian fluids (air and water), Equation (4) is employed while for the non-Newtonian fluids (sediment and earthfill dam), Equation (6) is used. The Navier-Stokes equations are discretized on a fixed Cartesian grid using the FVM method. The relationship between velocity and pressure is solved using an iterative method.

## NUMERICAL ALGORITHM

The PISO (Pressure-Implicit with Splitting of Operators) algorithm is chosen to solve the RANS equations (Eqs. 1-3 given in Section 2 above) numerically [49]. This is an extension of the SIMPLE method used to solve the Navier-Stokes equations. Generally the algorithm PISO takes less CPU time [44]. The PISO algorithm is a pressure velocity calculation procedure for the Navier-Stokes equations, originally developed for non-iterative calculation of the unsteady compressible flow, but it has been successfully adapted to the stationary problems [50]. The PISO algorithm contains one prediction step and two corrector steps and it is designed to ensure the mass conservation using the predictor-corrector steps. The algorithm can be simply summarized by the following steps [49]:

Step 1. The boundary conditions are set.

Step 2. The discrete momentum equation to calculate the intermediate velocity field is solved.

Step 3. The mass flows on the faces of the cells are calculated.

Step 4. The pressure equation is solved.

Step 5. The mass flows on the faces of the cell are corrected.

Step 6. The velocity based on the new pressure field is corrected.

Step 7. The boundary conditions are updated.

Step 8. Steps from Step 3 onward are repeated for specified number of times.

Step 9. The time step is increased and the steps from Step 1 onward are repeated.

The computational grid of the numerical model contained approximately 600,000 hexahedral cells. All the calculations were computed in PC: Intel Core i9, RAM 32 GB.

## VALIDATION OF THE NUMERICAL MODEL

Two experimental data herein are used for validating the developed numerical model.

**DAM BREAK FLOW OVER FIXED BED**

The numerical model is first verified using a laboratory measurement of a dam break flow on a fixed bed having an isolated block, conducted at the Netherlands Marine Research Institute (MARIN) [51]. The laboratory tank has the length of 3.22 m, the width of 0.993 m and the height of 1 m. A rectangular block with a size of 0.403 × 0.161 × 0.161 m is placed at 1.167 m downstream of the tank. The initial water depth inside the tank is 0.55 m, and the lower area is dry. Figure 1 displays the tank specification and the location of the gauges. Two water level meters (H2, H4) at the lower and upper positions of the movable gate, and four pressure gauges (P1, P3, P5, P7) on the side and upper parts of the block are installed. The details of the experiment can be obtained from Kleefsman et al. [51].

Figure 2 shows the temporary changes in the water levels at H4 and H2 sensors. As seen, the model captures the measured data. The water levels decrease at H4 up to 2.9 s, when the first reflected wave moves to the upper wall. The reflected wave contacts the wall and it is reflected back downstream, indicating a peak water level around 3.9 s. The front wave arrives at H2 in 0.4 s, and rises to 2.4 s when reflected waves arrive back from the block and the lower wall. The results are compatible with those in Cagatay and

Kocaman [3]. Table 1 summarizes the computed error measures for these simulations. As seen, the MAE and RMSE values are very low as 0.0072 m and 0.0182 m for H2 and 0.0077 m and 0.0245 m for H4, respectively.

The measured and simulated temporal change in the pressures at P1, P3, P5, P7 gauges are presented in Figure 3. As seen, there is sharp increase in the pressures at P1 and P3 when the wave hits the block at about 0.45 s. The simulated values show several false bursts on the sensors P5 and P7 due to air bubbles in the water and it is difficult for the model to cope with an isolated empty cell surrounded by fluid cells. Isolated empty cells occur when a progressive wave contacts the block, redirects upward and falls onto the

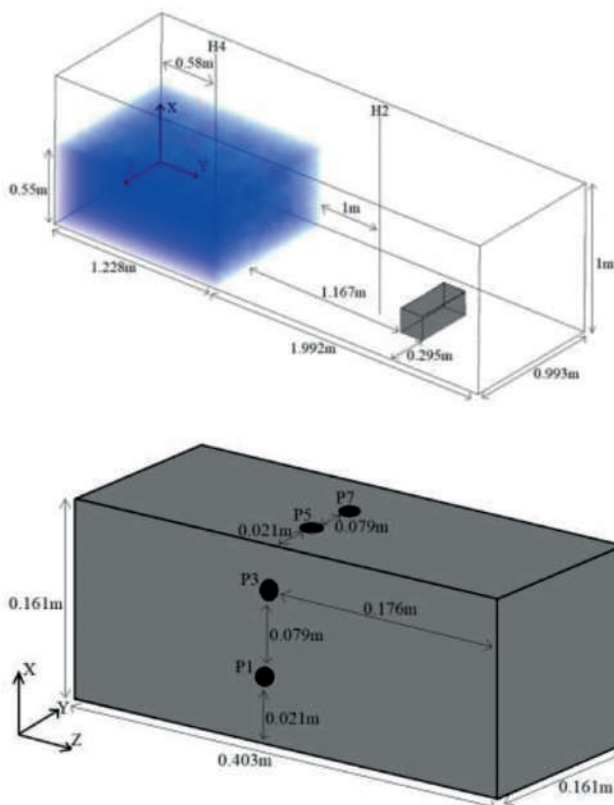


**Figure 1.** The computational geometry of the first laboratory measurement [51].

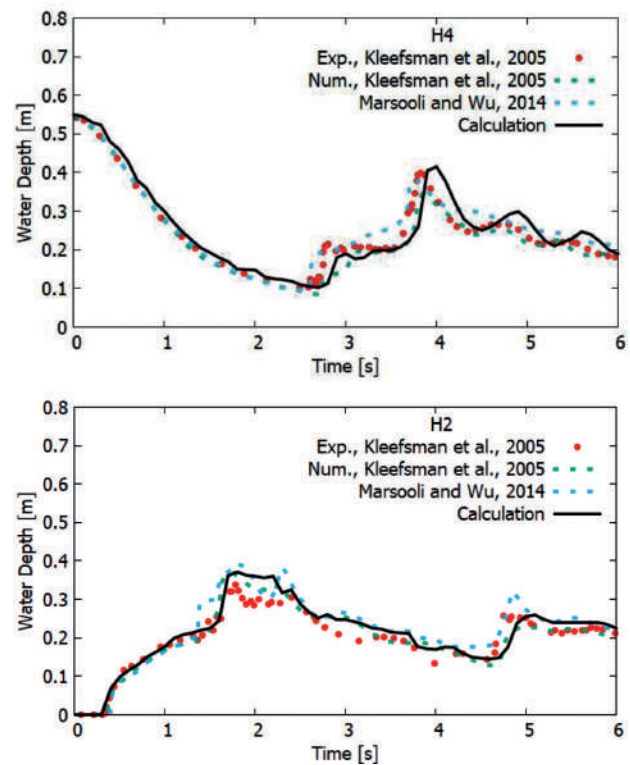


**Figure 2.** Measured and simulated water depths in the tank (H4) and at location H2.

**Table 1.** Error measures for simulations in Figures 2 and 3

	MAE	RMSE
P1 (Pa)	84.1	443.5
P3 (Pa)	74.7	313.8
P5 (Pa)	59.1	269.0
P7 (Pa)	112.3	394.6
H4 (m)	0.0077	0.0245
H2 (m)	0.0072	0.0182

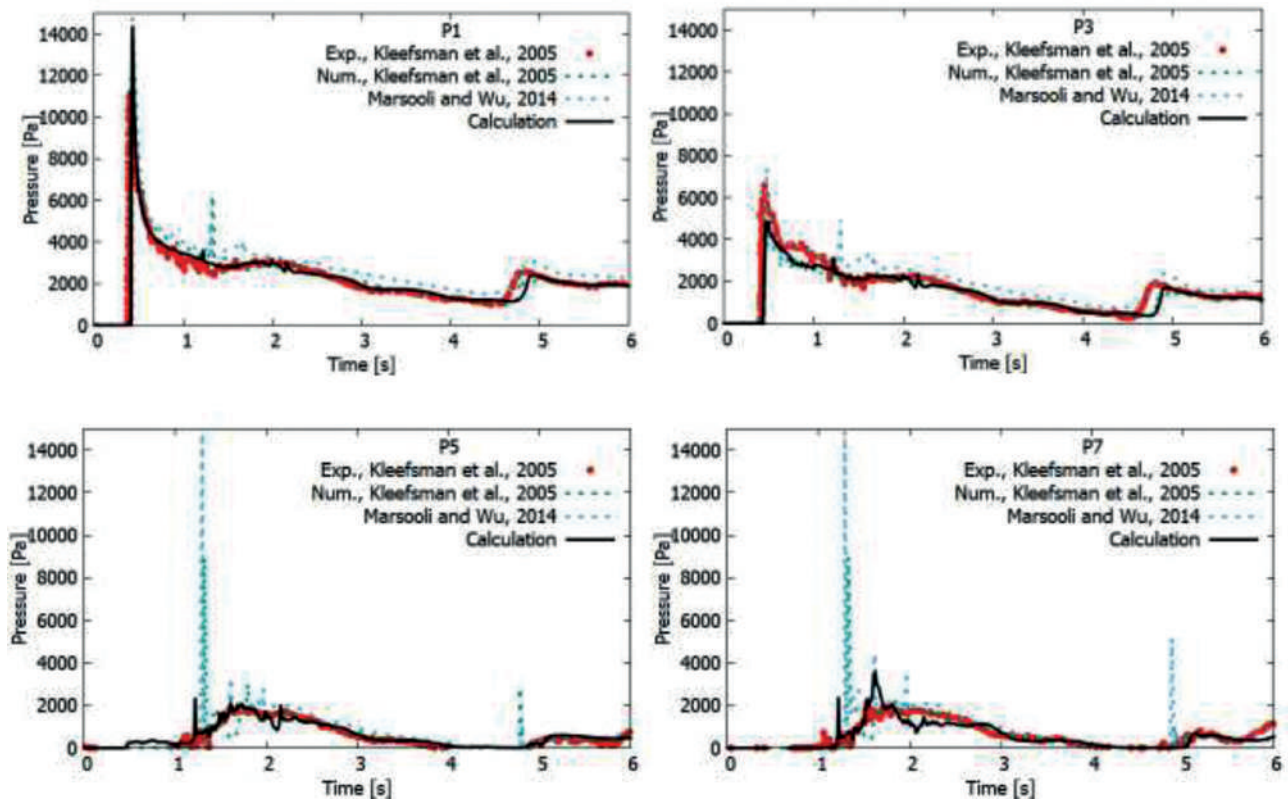


Figure 3. Comparison of predicted and measured pressures at various pressure gauges (P1, P3, P5 and P7).

top of the block. The same case is also shown elsewhere [51] and [52]. However, the comparisons in Figure 3 show that the developed model has a good ability to predict the temporal change in the pressures. It is especially worth noting that a very good prediction is done at location P1. Table 1 summarizes the computed error measures for these simulations. As seen, the MAE and RMSE values are, on the average, very low as 82.2 Pa and 355.2 Pa, respectively.

Figure 4 displays the early stages of two snapshots of the simulation, together with the images from the laboratory experimental measurements of Kleefsman et al. [51]. As seen, there is a good match between the snapshots of the simulations and the experiments, especially when water first hits the block at 0.4 sec and 0.56 s. The obtained numerical simulation results are in good agreement with the measurement data with regard to the capturing of the wave front, arrival times, and pressures. They are also compatible with those in Cagatay and Kocaman [3].

### DAM BREAK FLOW OVER A MOVING BED

The second test case involves the applicability of the developed model when the dam break water flows over a movable bed. The obtained computational values are compared against the measured data and the predicted values

given in Soares-Frazão et al. [53]. The geometry of the region in which the calculations are performed is shown in Figure 5. The width of the reservoir section of the flume is 3.6 m and the narrow section of the flume is 1 m. The fixed base of the channel is covered with coarse and saturated sand layers at a height of 0.085 m. In the laboratory measurements, homogeneous coarse sand  $\rho_s / \rho_w = 2.63$  is used. The model for the sediment phase is considered as the non-Newtonian fluid. The water height in the reservoir at the initial stage is 0.47 m. Figure 5 also shows the control points where the hydrometric measurements are carried out. The coordinates of the control points are given in Table 2. The details of the experiment can be obtained from Soares-Frazão et al [53].

Figure 6 shows the calculated values of changes in the water levels at the control points and their comparisons against the experimental and computational values given in Soares-Frazão et al [53]. As seen, the obtained numerical data are comparable with the experimental data. The cause of some deviations may be due to conditions associated with the characteristics of the sedimental environment, as well as the surface roughness coefficients and the initial conditions. The presence of a mobile bed (non-Newtonian fluid) assists to decrease the flow rate and influence the transport in general. This implies that in the case of dam

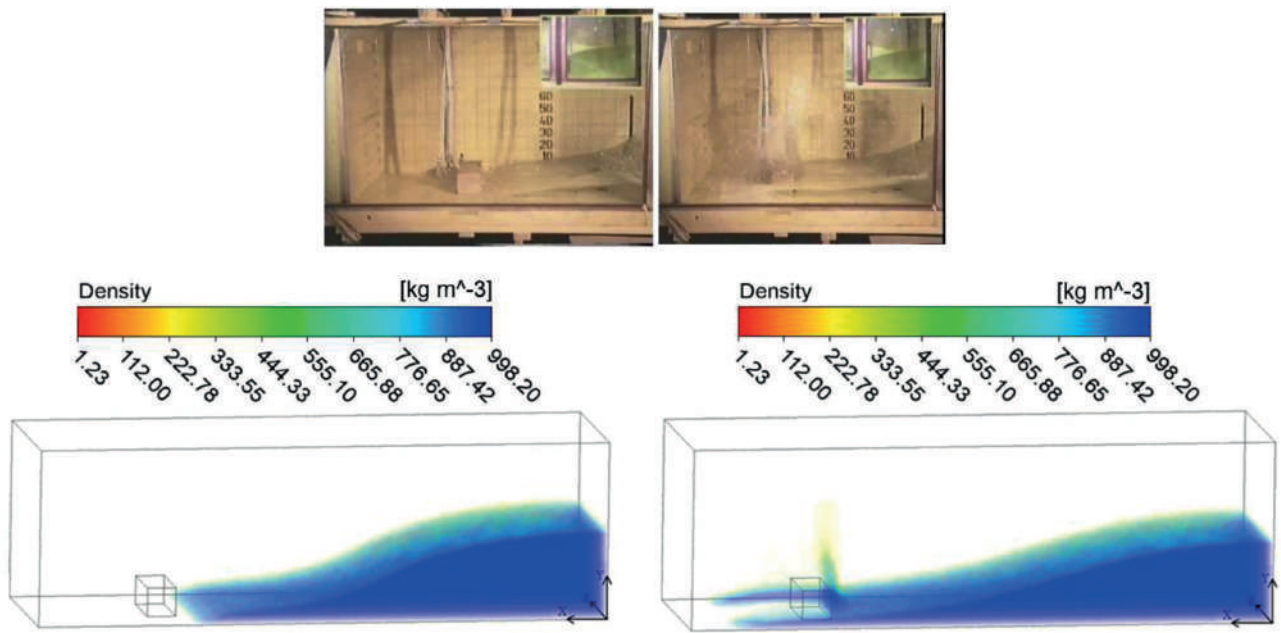


Figure 4. Images of modeling dam break flood waves at 0.4 s and 0.56 s of the experiments (the top picture is from the actual laboratory experiments of Kleefsman et al. [51]).

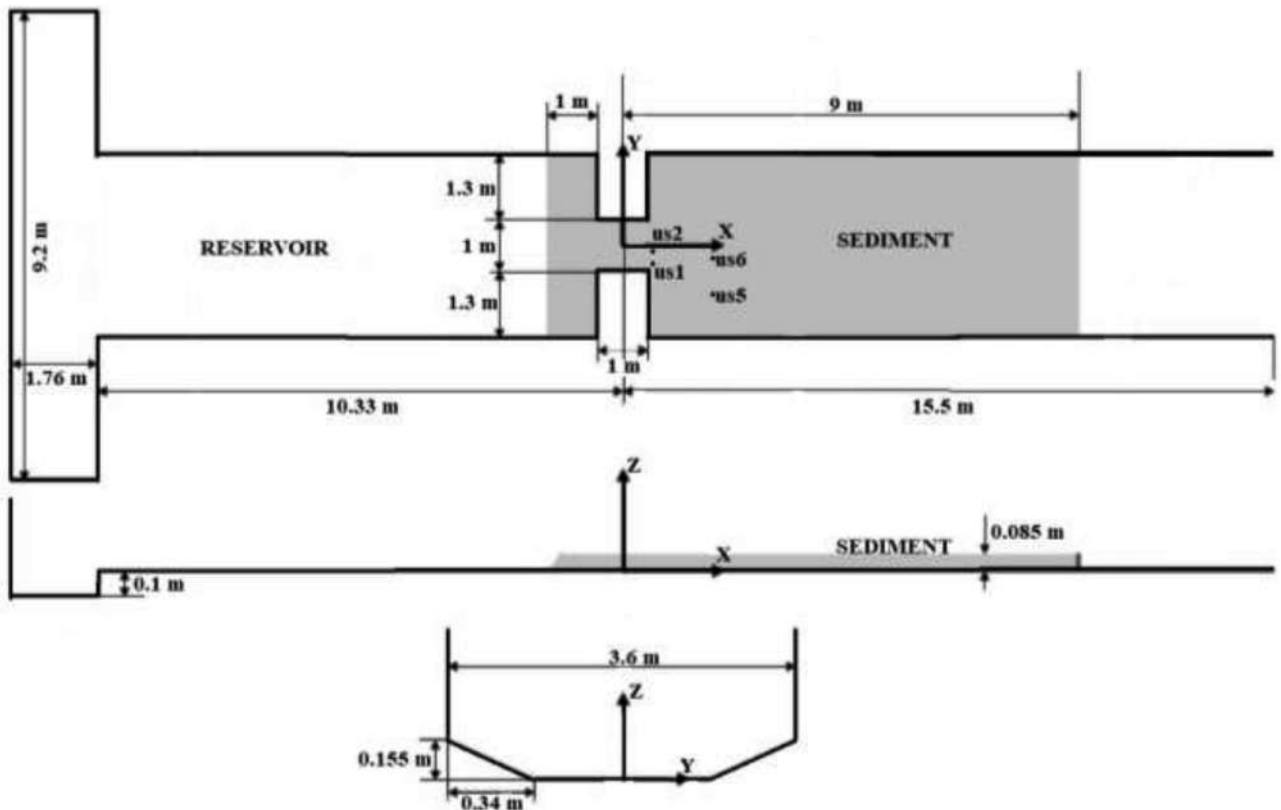


Figure 5. Plan view of the second laboratory experimental set-up [53].

**Table 2.** Coordinates of the sensors [53]

Measuring detectors	X - axis	Y-axis
Us1	64 cm	-50 cm
Us2	64 cm	-16.5 cm
Us5	194 cm	-99 cm
Us6	194 cm	-33cm

failure, sediment deposits can increase at the immediate dam vicinity [17] and [54].

Figure 7 displays the three dimensional water flow profiles at different periods of the simulation. As seen, the model has produced reasonable numerical simulations of the water flow over a movable sediment bed. From the results of this test problem, it can be concluded that the presence of a movable layer can have a significant effect on the movement of the flow during a dam break. In particular, differences in behavior are noticeable at the initial stages of the break, as well as during the first collision of the flow with the obstacle.

**APPLICATION OF THE NUMERICAL MODEL**

**Earthfill Dam Break Over a Fixed Bed**

In each experiment given in Section 4, the dam body is resembled with a movable metal gate. However, in real life conditions, earthfill dam bodies are constructed from bulk of sediments. Therefore, in this section, simulations of water and sediment transport due to an earthfill dam failure is investigated. For this purpose, the first experimental model (see Fig.1) given in Figure 8A is artificially conceptualized as the one in Figure 8B where the dam body is considered to be formed as a bulk of sediment in the shape of a triangle. All the corresponding dimensions of the region, the location of the sensors, and the location of the obstacle remain the same as in the first experimental problem, presented in Section 4. All the sizes of the studied area remain the same as in the first experiment and the volume of water in the tank has changed due to the artificial dam body. The conceptualized triangle bulk dam body has the height of 0.55 m, with a base width of 0.294 m. Homogeneous coarse sand used in the laboratory measurements is considered herein with the same density ratio ( $\rho_s / \rho_w = 2.404$ ) and a coarse grain density sand is set to 2400 kg/m<sup>3</sup>. The coarse sand model is considered as the non-Newtonian fluid. The effective viscosity for the non-Newtonian fluid is calculated by Eq. (7). The water height in the reservoir at the initial moment is assumed to be the same as 0.55 m.

Figure 9 displays the comparison of the temporal changes at P1, P3, P5 and P7 between the A and B laboratory conceptualizations and the corresponding experimental measurements and the computations given in Marsooli and Wu [52] and Kleefsman et al [51]. As seen in Figure 9, there is a noticeable decrease in the shock pressure at all

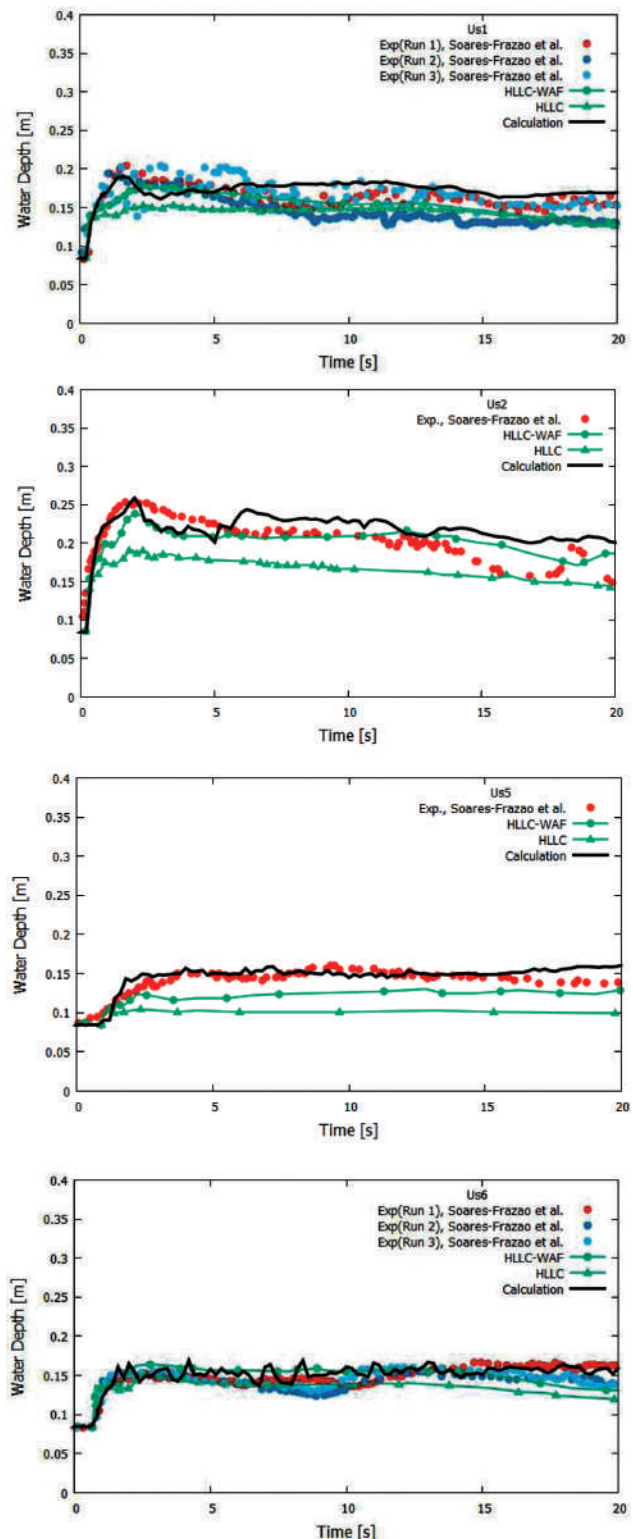


**Figure 6.** Comparison of the model results against the laboratory measurements from Soares-Frazão et al. [53] for the water surface profile at different points (Us1, Us2, Us5, Us6) (HLLC is the dam break solver: Harten-Lax-van Leer-Contact, and WAF: is the dam break solver: Weighted Average Flux).

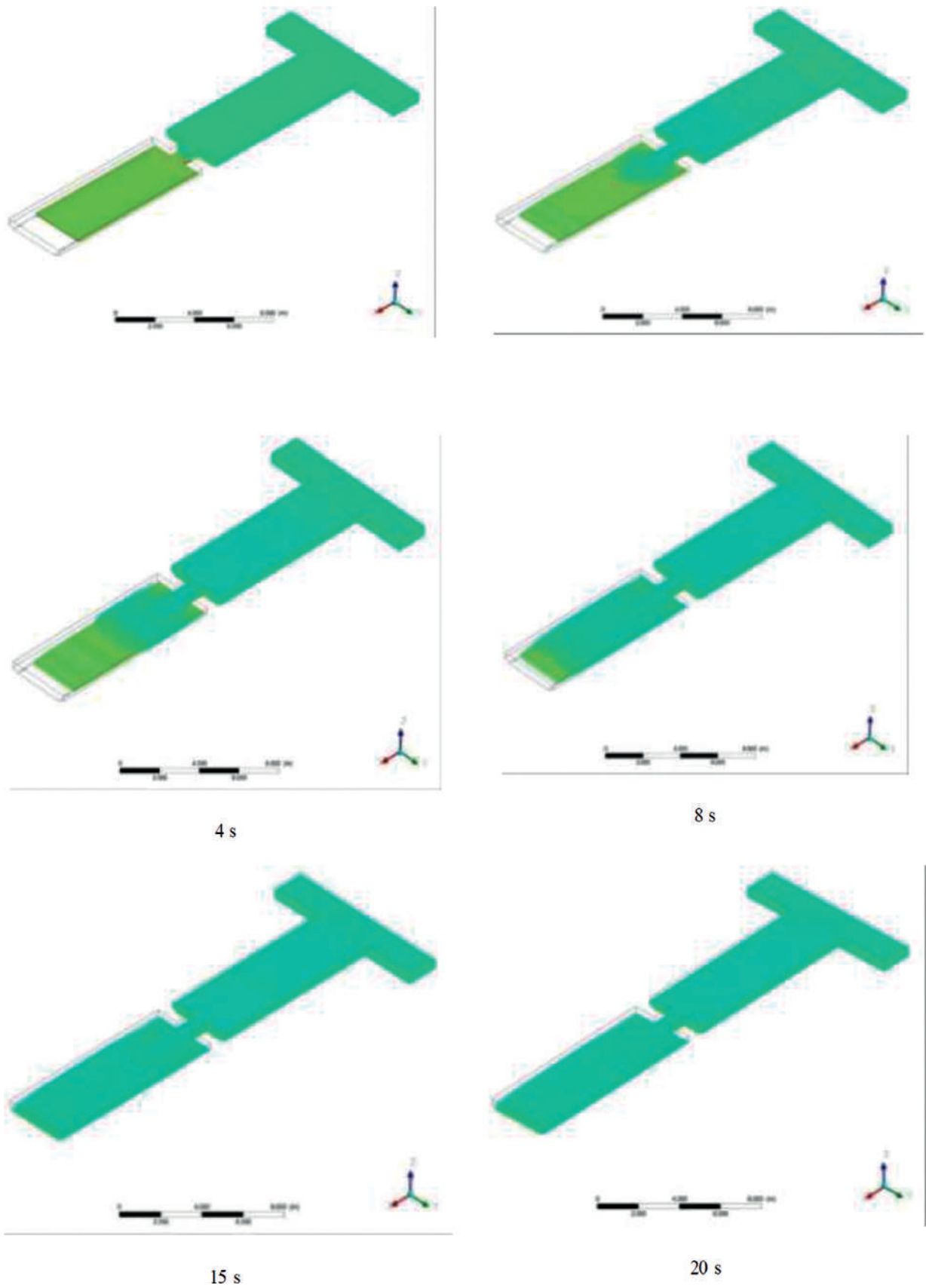


Figure 7. Water flow over a movable sediment bed at different times of the simulation between  $t = 0$ -20 s.

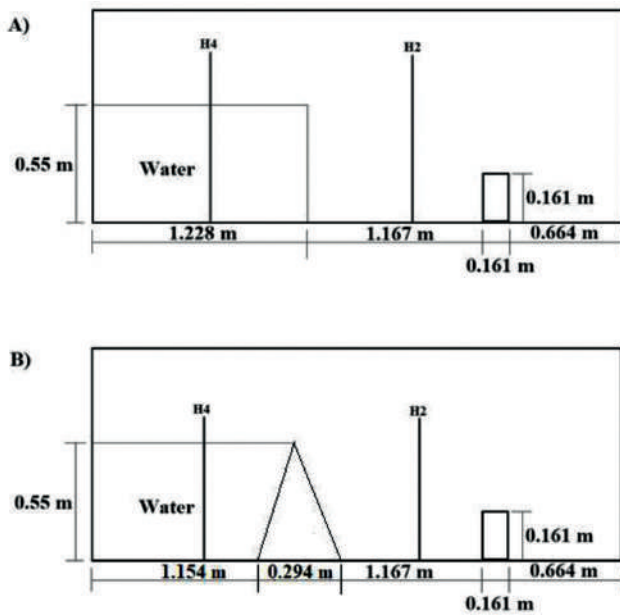


Figure 8. Conceptualized dam break experiment: A. the dam body is a movable metal [51] and B. the dam body is bulk of sediment.

points (P1, P3, P5, and P7). This is because the sediment movement within the water flow reduces the flow velocity. The slowness in the flow can also be noticed by the arrival time of the flow at the measuring points. However, it is worth noting that the pressures at all points after 2.5 seconds for the problem B are higher than those for the problem A, since in general the flow becomes calmer after 2.5 s and the influence of the propagation on the velocity becomes less than the mass forces.

Comparisons of the flow levels are presented in Figure 10. As seen, the levels of flooding at H4 and H2 are noticeable different for the conceptualizations A and B. The main difference is that in the formulation B, the flow is relatively calmer and the levels of flooding at some time intervals are higher due to the existence of the sediment.

Figure 11 illustrates the effect of bulk dam body sediment movement together with the water flow. As seen, the bulk dam body sediment moves together with the water flow while at the same time spreading. Both water and bulk sediment fronts reach to the obstacle at 0.7 s and top it at 1 s of the simulation. By 2 s of the simulation, we see the spreading of the sediment wave at both upstream and downstream sides of the obstacle. The water wave front

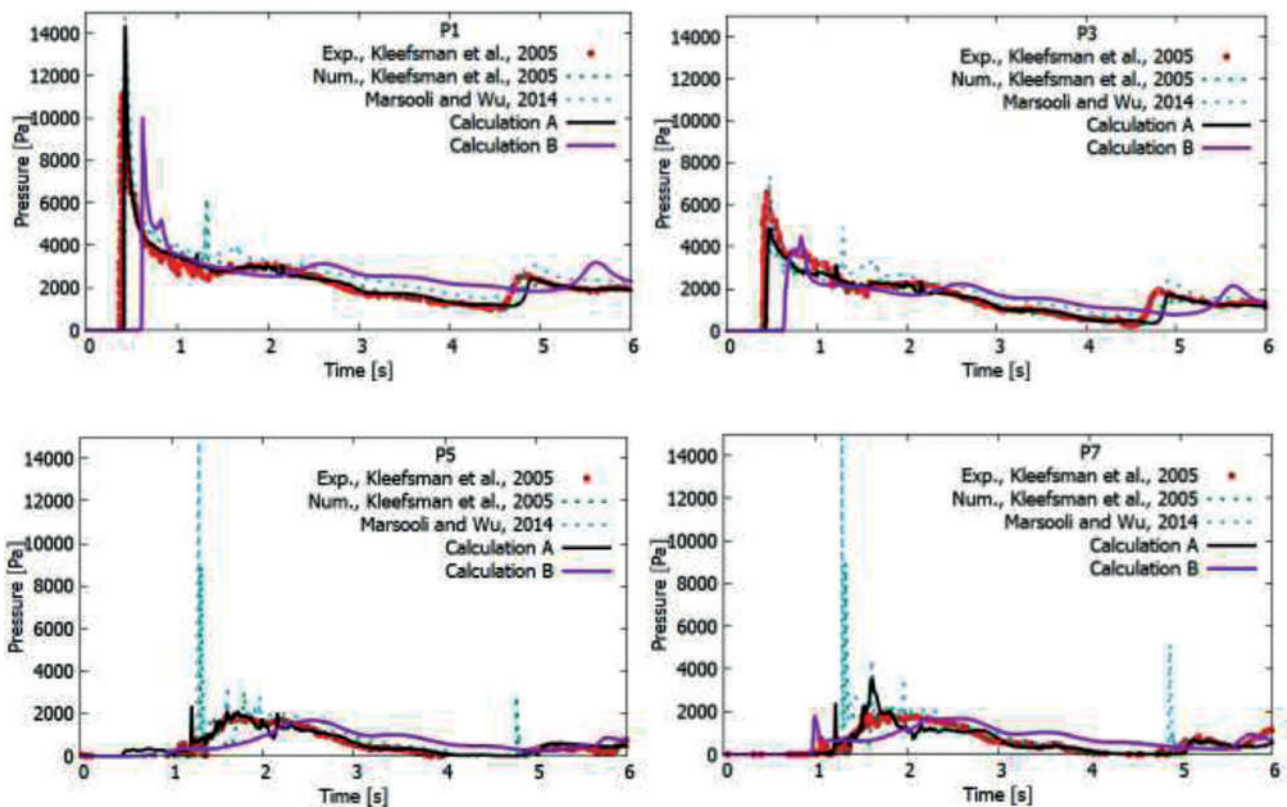


Figure 9. Pressure profiles on pressure gauges P1, P3, P5 and P7.

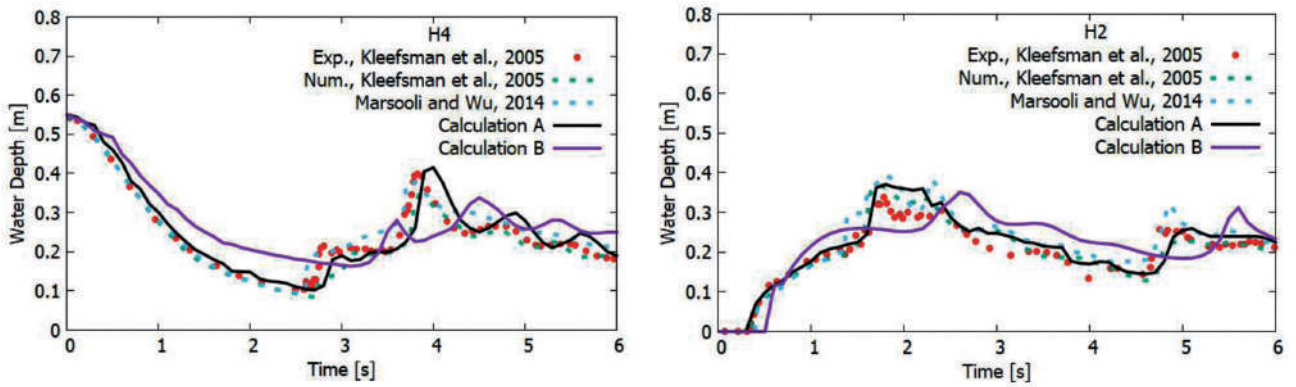


Figure 10. Simulated and measured water depths at H4 and H2 level meters.

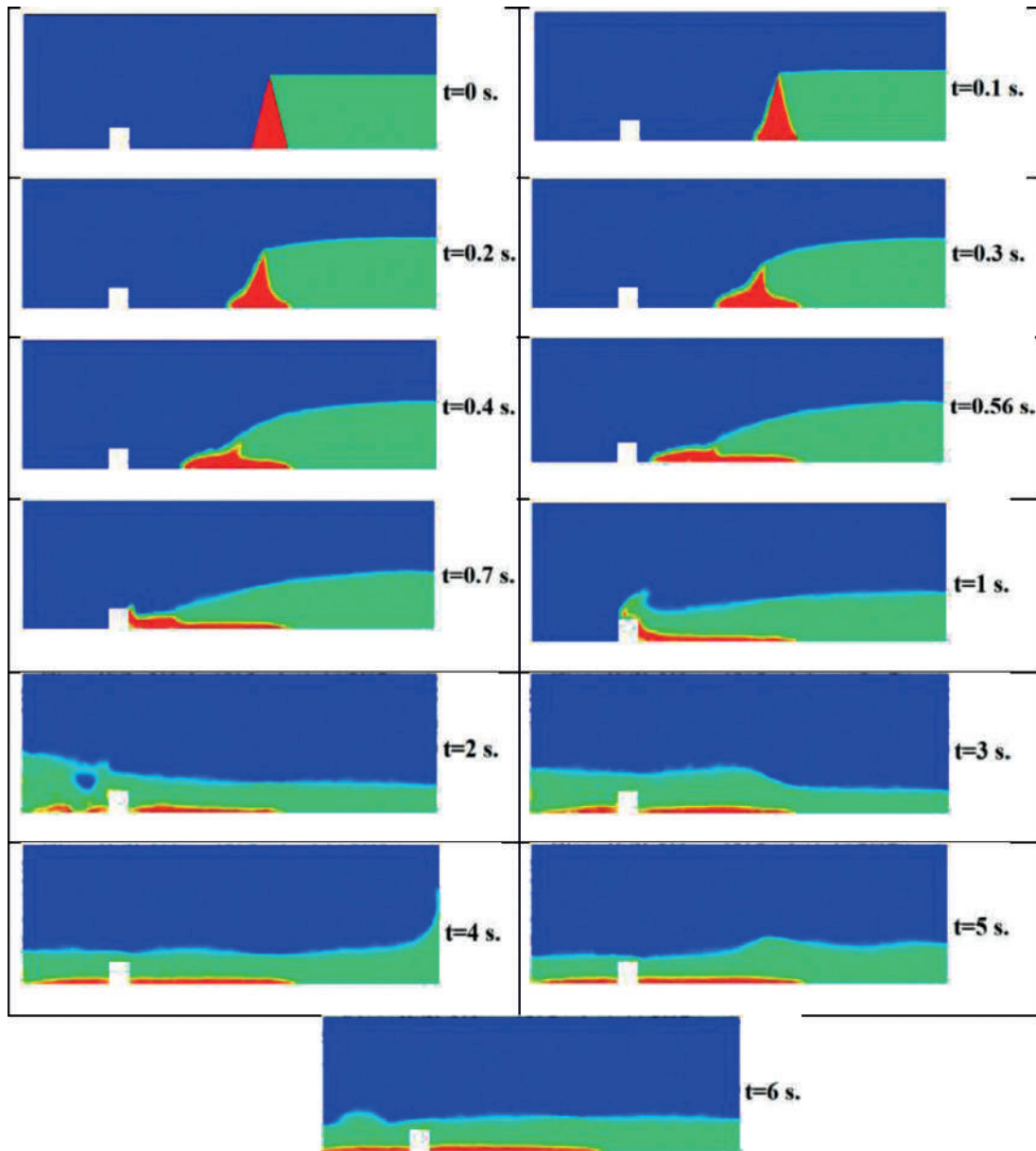
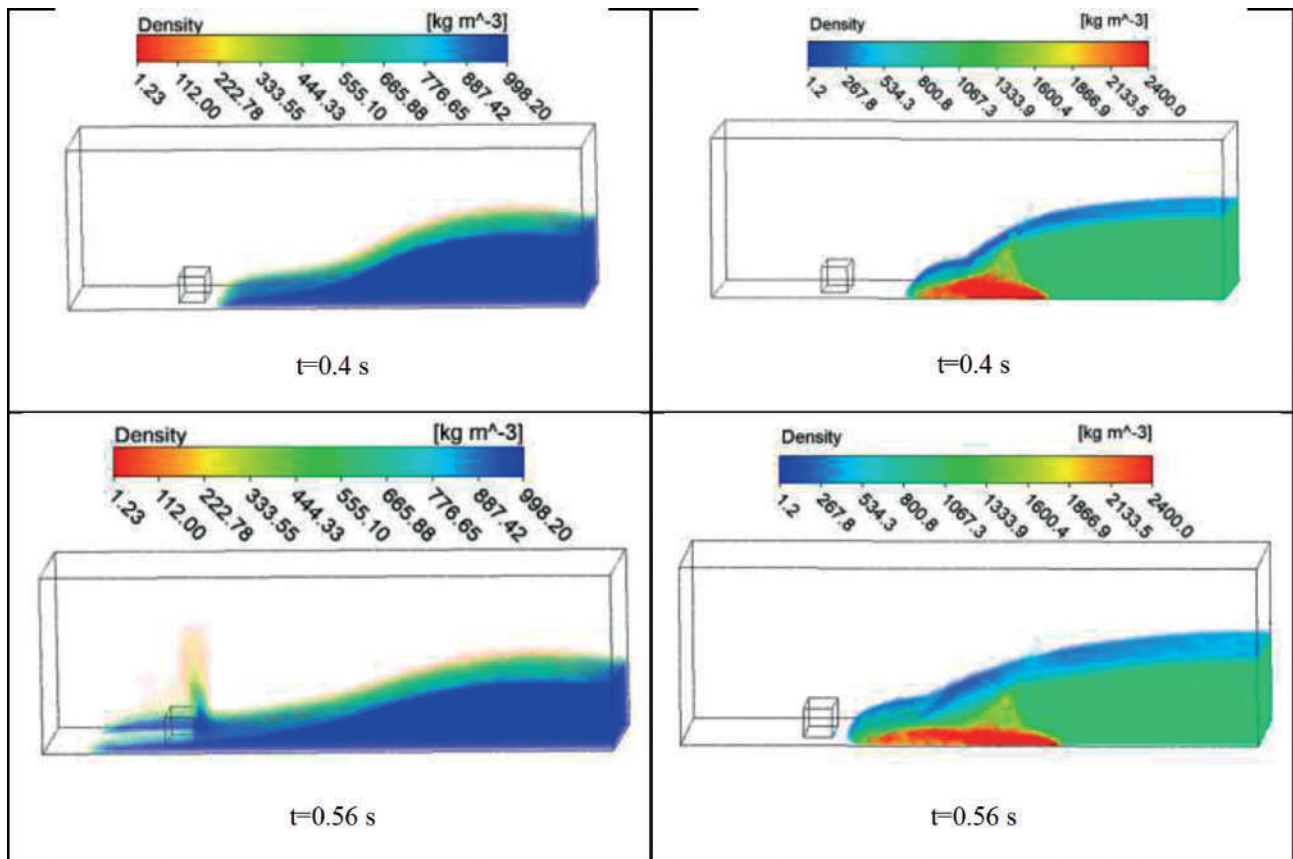


Figure 11. Two-dimensional profiles of the flow at different locations in time.



**Figure 12.** Comparison of images from modeling of a dam break without and with bulk soil dam for different times with an obstacle.

position is almost the same as the sediment wave front at the beginning of the dam break, yet then, in time, the flow is mixed with the sediment influencing the wave front leading to the inhibition which can be easily observed in front of the obstacle after 0.56 s (Figures 11 and 12). Figure 12 shows the three dimensional movement of water for the case A and water and sediment for the case B. As seen, it takes longer time for sediment laden flow to reach the obstacle, as expected. These results are in agreement with the literature [3] and [17].

**EARTHFILL DAM BREAK OVER A MOVING BED**

To study the influence of the dam body soil type on the dam break flow and sediment transport over a moving bed, three scenarios are considered for the second experimental setting (Figure 13). The basic formulation and dimensions of the second experiment remain the same, with the exception of the dam body. The reservoir has the width of 3.6 m and the length of 36.0 m, of which about 27.6 m is usable. The coordinates are taken at the center of the dam body. The flume bed is covered with coarse and saturated sand layers at a height of 0.085 m. The total coating length is 10.0

**Table 3.** Three different soil type densities

Scenario	Density (kg/m3)
1	2630
2	3000
3	3300

m, while the length of channel 1.0 m before the narrow section and 9 m after the narrow section. In this experimental set up, the movable bed is considered to be formed from sand with the density ratio of  $\rho_s / \rho_w = 2.6$ . In each scenario, different soil density is considered in the dam body (Table 3). Figure 13 also shows the control points at which the hydrometric measurements are carried out. The coordinates of the control points are given in Table 2.

The simulations for the three scenarios are presented in Figure 14, where the flow levels at the four sensors are compared. As seen, the flow levels at the sensors initially increase due to the presence of a portable bulk dam. At the initial moment of the dam break, the dam body soil is transferred due to the pressure of the flow. The dam

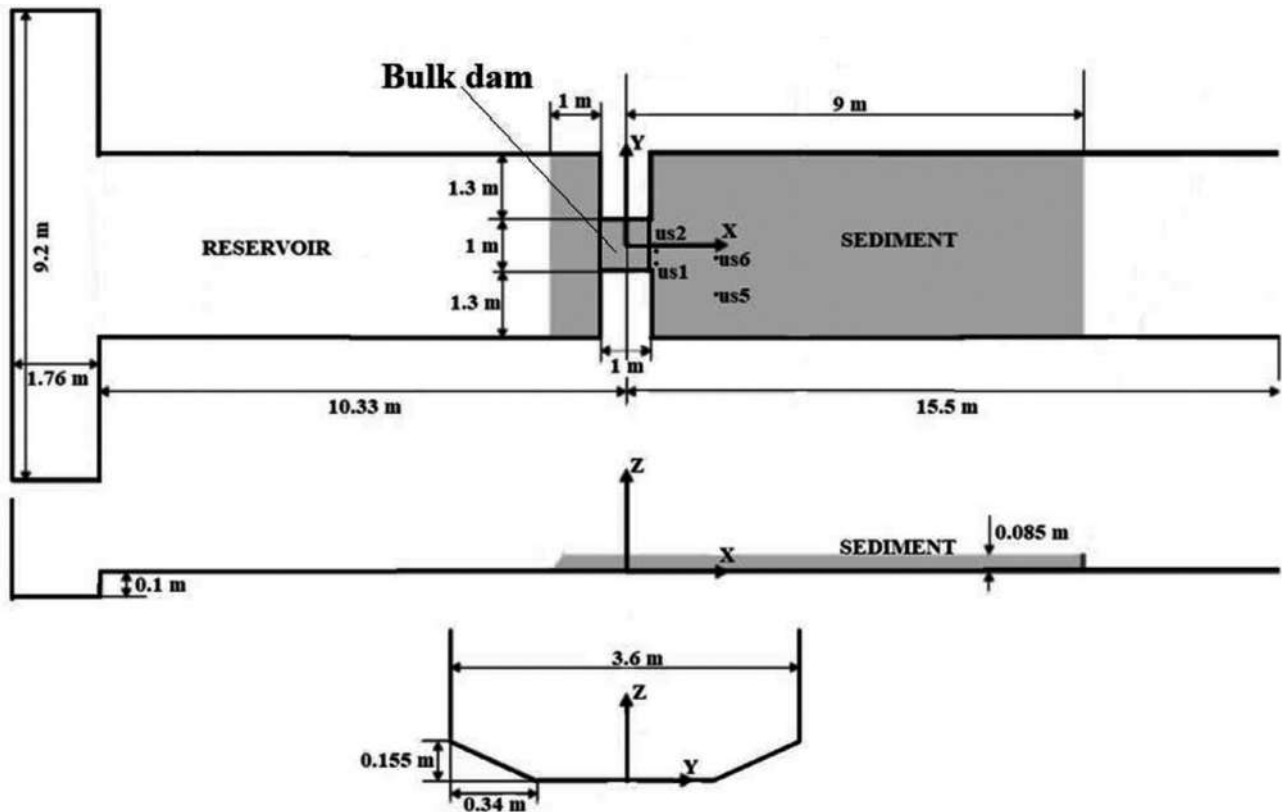


Figure 13. Considered experimental setup for studying the influence of dam body soil type [53].

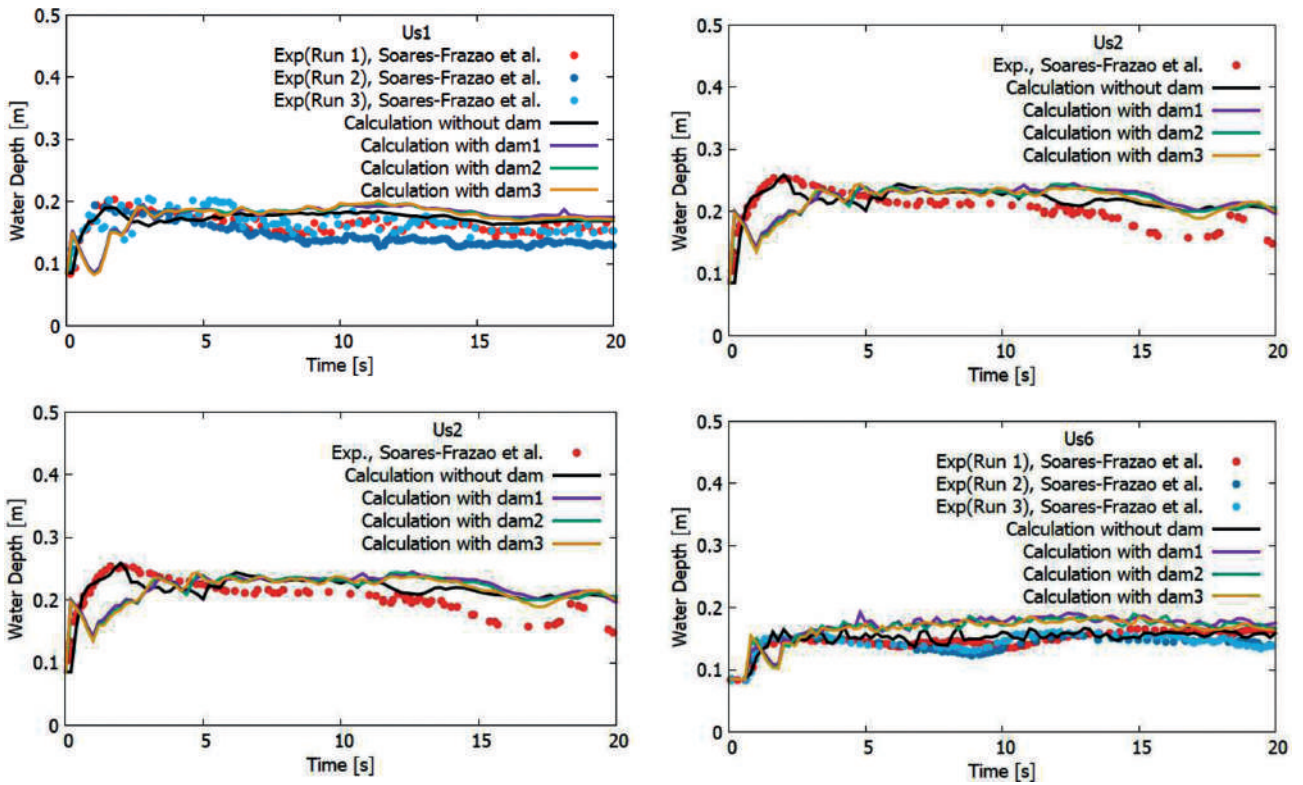
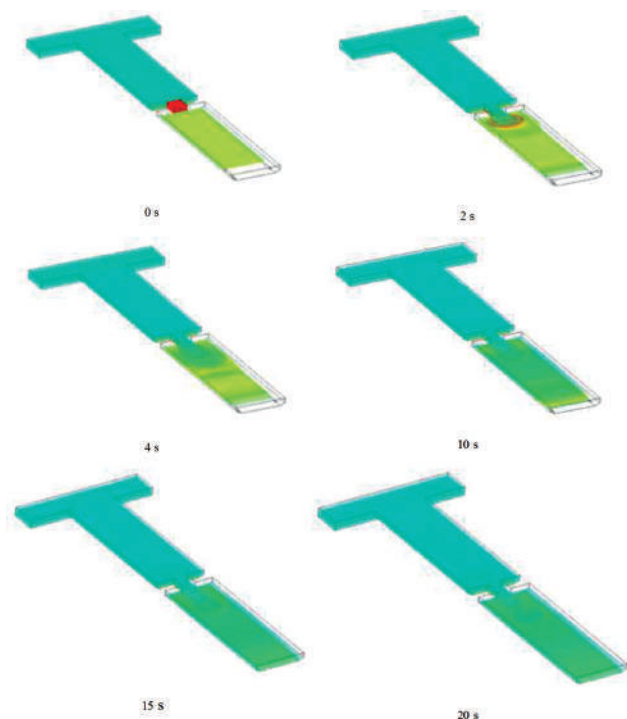


Figure 14. Measured and simulated water depths at Us1, Us2, Us5, Us6.



**Figure 15.** Three-dimensional images of a breakthrough at different points in time.

body sediment transport as a whole slows down the flow. However, it should be noted that, in general, the transport behavior under the three scenarios (three different soil type) is very similar. This similarity is due to the relatively small volume of the bulk dam compared to the volume of water.

Three-dimensional images of the transport at different times for the third scenario are presented in Figure 15. As seen, the collapsed part of the dam is transported downstream and settles in a wider channel. An enormous section of the movable bed is transported to a wide section of the channel and it starts to slowly settle in the region and forms a newly terrain. This phenomenon initiates further modification in the terrain, and also leads to a general change in the channel. These results indicate that the collapsing and consequently moving sediment can significantly increase the depth of flooding and change the morphology of the downstream area.

## CONCLUSIONS

This paper presents the results of the modeling flow and sediment transport due to an earthfill dam break. The modelling is accomplished by using the VOF method for the multiphase flow. The phase characteristic parameter is used; as phases of air, water, sediment, and bulk of dam body. The system of equations are solved numerically using the PISO algorithm.

The reliability of the proposed numerical method is verified by two test problems with the laboratory data. The model successfully captured the temporal changes in the measured flow depths, pressures, wave fronts, and the arrival times. These results illustrate the effectiveness of the proposed numerical method.

Two application problems are considered: (1) the dam body is considered having a bulk sediment in the shape of a triangle and the downstream section has a fixed bed and an obstacle, and (2) the dam body is considered to be formed by a different soil and a movable downstream bed. The simulations showed that, due to sediment, there is a noticeable decrease in the shock pressure at all points around the obstacle and there is an increase in the water levels. The bulk dam body sediment moves together with the water flow while spreading. It takes longer time for the sediment laden flow to reach the obstacle, as compared the clear water case. The soil type has minor effect while the transport of sediment can raise the water levels and change the morphology of the downstream section.

The presented modeling results demonstrate the importance of taking into account the transport of the dam body sediment since these can significantly affect the flow by changing direction and magnitude. The dam body sediment transport as a whole slows down the flow. It can cause a deformation in the terrain. On the other hand, it can slow down the wave front since it would increase the density and viscosity of the mixture. In general, it seems that the soil type has minor effect on the transport behavior. The developed numerical model can be useful for realistically modelling the three dimensional non-Newtonian fluid transports due to an earthfill dam breaks over complex terrains.

It needs to be pointed out that, in this study, the conceptualized earthfill dam break simulations are carried out. The conceptualized dam bodies (movable metal gate and/or triangular sediment) cannot be encountered in real world applications. Although the numerical simulations under such circumstances can be useful with regard to investigating the behavior and transport of flow and sediment and thus consequently gaining an insight into the physics of the processes, the applications of the developed numerical model on real world dam body failures could be very beneficial to show the effectiveness of the model.

## AUTHORSHIP CONTRIBUTIONS

Authors equally contributed to this work.

## DATA AVAILABILITY STATEMENT

The authors confirm that the data that supports the findings of this study are available within the article. Raw data that support the finding of this study are available from the corresponding author, upon reasonable request.

## CONFLICT OF INTEREST

The author declared no potential conflicts of interest with respect to the research, authorship, and/or publication of this article.

## ETHICS

There are no ethical issues with the publication of this manuscript.

## REFERENCES

- [1] Albu LM, Enea A, Iosub M, Breaban IG. Dam Breach Size Comparison for Flood Simulations. A HEC-RAS Based, GIS Approach for Drăcșani Lake, Sitna River, Romania. *Water* 2020;12:1090. [\[CrossRef\]](#)
- [2] Macchione F. Model for predicting floods due to earthen dam breaching. I: Formulation and evaluation. *J Hydraulic Eng* 2008;134:1688–1696. [\[CrossRef\]](#)
- [3] Cagatay HO, Kocaman, S. Dam-break flow in the presence of obstacle: Experiment and CFD simulation. *Eng Appl Comput Fluid Mech* 2011;5:541–552. [\[CrossRef\]](#)
- [4] Hu H, Zhang J, Li T, Yang J. A simplified mathematical model for the dam-breach hydrograph for three reservoir geometries following a sudden full dam break. *Nat Hazards* 2020;102:1515–1540. [\[CrossRef\]](#)
- [5] Fadaee M, Kermani MZ. Experimental study and numerical simulation of dam reservoir sediment release. *Water SA* 2020;46:656–664. [\[CrossRef\]](#)
- [6] Aliparast M. Two-dimensional finite volume method for dam-break flow simulation. *Int J Sediment Res* 2009;24:99–107. [\[CrossRef\]](#)
- [7] Singh J, Altinakar MS, Ding Y. Two-dimensional numerical modeling of dam-break flows over natural terrain using a central explicit scheme. *Adv Water Resour* 2011; 34, 1366–1375. [\[CrossRef\]](#)
- [8] Oertel M, Bung DB. Initial stage of two-dimensional dam-break waves: laboratory versus VOF. *J. Hydraul Res* 2012;50:89–97. [\[CrossRef\]](#)
- [9] Qi H, Altinakar M. GIS-based decision support system for dam break flood management under uncertainty with two-dimensional numerical simulations. *J Water Resour Plann Manag* 2012;138:334–341. [\[CrossRef\]](#)
- [10] LaRocque LA, Imran J, Chaudhry MH. Experimental and numerical investigations of two-dimensional dam-break flows. *J Hydraulic Eng* 2013;139:569–579. [\[CrossRef\]](#)
- [11] Haltas I, Elçi S, Tayfur G. Numerical simulation of flood wave propagation in two-dimensions in densely populated urban areas due to dam break. *Water Res Manag* 2016;30:5699–5721. [\[CrossRef\]](#)
- [12] Haltas I, Tayfur G, Elçi S. Two-dimensional numerical modeling of flood wave propagation in an Urban area due to Ürkmez Dam-Break, İzmir, Turkey. *Nat Hazards* 2016;81:2103–2119. [\[CrossRef\]](#)
- [13] Guney MS, Tayfur G, Bombar G, Elçi S. Distorted physical model to study sudden partial dam break flows in an urban area. *J Hydraul Eng* 2014;140:05014006. [\[CrossRef\]](#)
- [14] Marsooli R, Wu W. 3-D finite-volume model of dam-break flow over uneven beds based on VOF method. *Adv Water Res* 2014;70:104–117. [\[CrossRef\]](#)
- [15] Wang X, Chen W, Zhou Z, Zhu Y, Wang C, Liu Z. Three-dimensional flood routing of a dam break based on a high-precision digital model of a dense urban area. *Nat Hazards* 2017;86:1147–1174. [\[CrossRef\]](#)
- [16] Oguzhan S, Ozgenc AA. Experimental investigation of the effect of vegetation on dam break flood waves. *J Hydrol Hydromech* 2020;3:231–241. [\[CrossRef\]](#)
- [17] Munoz DH, Constantinescu G. 3-D dam break flow simulations in simplified and complex domains. *Adv Water Res* 2020;137:103510. [\[CrossRef\]](#)
- [18] Kocaman S, Dal K. A new experimental study and SPH comparison for the sequential dam-break problem. *J Marine Sci Eng* 2020;8:905. [\[CrossRef\]](#)
- [19] Wang B, Liu W, Wang W, Zhang J, Chen Y, Peng Y, et al. Experimental and numerical investigations of similarity for dam-break flows on wet bed. *J Hydrol* 2020;583:124598. [\[CrossRef\]](#)
- [20] Turhan E, Ozmen-Cagatay H, Kocaman S. Experimental and numerical investigation of shock wave propagation due to dam-break over a wet channel. *Polish Environ Stud* 2019;28:2877–2898. [\[CrossRef\]](#)
- [21] Stolle J, Ghodoosipour B, Derschum C, Nistor I, Petriu E, Goseberg N. Swing gate generated dam-break waves. *J Hydraulic Res* 2019;57:675–687. [\[CrossRef\]](#)
- [22] Gingold RA, Monaghan JJ. Smoothed particle hydrodynamics: theory and application to non-spherical stars. *Mon Not R Astron Soc* 1977;181:375–389. [\[CrossRef\]](#)
- [23] Idelsohn SR, Oñate E, Calvo N, Del Pin F. The meshless finite element method. *Int J Numer Methods Eng* 2003;58:893–912. [\[CrossRef\]](#)
- [24] Idelsohn SR, Oñate E, Pin FD. The particle finite element method: a powerful tool to solve incompressible flows with free-surfaces and breaking waves. *Int J Numer Methods Eng* 2004;61:964–989. [\[CrossRef\]](#)
- [25] Liu MB, Liu GR, Zong Z. An overview on smoothed particle hydrodynamics. *Int J Comput Methods* 2008;05:135–188. [\[CrossRef\]](#)
- [26] Tang ZY, Zhang YL, Wan DC. Numerical simulation of 3-D free surface flows by overlapping MPS. *J Hydrodynamics* 2016;28:306–312. [\[CrossRef\]](#)
- [27] Zhang AM, Sun PN, Ming FR, Colagrossi A. Smoothed particle hydrodynamics and its

- applications in fluid-structure interactions. *J Hydrodynamics* 2017;29:187–216. [\[CrossRef\]](#)
- [28] Sun P, Zhang AM, Marrone S, Ming F. An accurate and efficient SPH modeling of the water entry of circular cylinders. *Appl Ocean Res* 2018;72:60–75. [\[CrossRef\]](#)
- [29] Rezavand R, Zhang C, Hu X. A weakly compressible SPH method for violent multi-phase flows with high density ratio. *J Comput Phys* 2019;402:109092. [\[CrossRef\]](#)
- [30] Larsson S, Prieto JMR, Gustafsson G, Haggblad HA, Jonsen P. The particle finite element method for transient granular material flow: modelling and validation. *Comput Part Mech* 2021;8:135–155. [\[CrossRef\]](#)
- [31] Sussman M, Smith KM, Hussaini MY, Ohta M, Zhi-Wei R. A sharp interface method for incompressible two-phase flows. *J Comput Phys* 2007;221:469–505. [\[CrossRef\]](#)
- [32] Olsson E, Kreiss G, Zahedi S. A conservative level set method for two phase flow II. *J Comput Phys* 2007;225:785–807. [\[CrossRef\]](#)
- [33] Wang Z, Yang J, Koo B, Stern F. A coupled level set and volume-of-fluid method for sharp interface simulation of plunging breaking waves. *Int J Multiph Flow* 2009;35:227–246. [\[CrossRef\]](#)
- [34] Shukla RK, Pantano C, Freund JB. An interface capturing method for the simulation of multi-phase compressible flows. *J Comput Phys* 2010;229:7411–7439. [\[CrossRef\]](#)
- [35] Billaud M, Gallice G, Nkonga B. A simple stabilized finite element method for solving two phase compressible–incompressible interface flows. *Comput Method Appl Mech Eng* 2011;200:1272–1290. [\[CrossRef\]](#)
- [36] Zhao L, Mao J, Bai X, Liu X, Li T, Williams JJR. Finite element implementation of an improved conservative level set method for two-phase flow. *Comput Fluids* 2014;100:138–154. [\[CrossRef\]](#)
- [37] Montazeri H, Zandavi SH, Bazylak A. Sharp interface models for two-phase flows: insights towards new approaches. *Comput Method Appl Mech Eng* 2017;322:238–261. [\[CrossRef\]](#)
- [38] Hirt CW, Nichols BD. Volume of fluid (VOF) method for the dynamics of free boundaries. *J Comput Phys* 1981;39:201–225. [\[CrossRef\]](#)
- [39] Gueyffier D, Li J, Nadim A, Scardovelli R, Zaleski S. Volume-of-Fluid interface tracking with smoothed surface stress methods for three-dimensional flows. *J Comput Phys* 1999;152:423–456. [\[CrossRef\]](#)
- [40] Pilliod JE, Puckett EG. Second-order accurate volume-of-fluid algorithms for tracking material interfaces. *J Comput Phys* 2004;199:465–502. [\[CrossRef\]](#)
- [41] Gerlach D, Tomar G, Biswas G, Durst F. Comparison of volume-of-fluid methods for surface tension-dominant two-phase flows. *Int J Heat Mass Transf* 2006;49:740–754. [\[CrossRef\]](#)
- [42] Seric I, Afkhami S, Kondic L. Direct numerical simulation of variable surface tension flows using a volume-of-fluid method. *J Comput Phys* 2018;352:615–636. [\[CrossRef\]](#)
- [43] Nguyen VT, Nguyen NT, Phan TH, Park WG. Efficient three-equation two-phase model for free surface and water impact flows on a general curvilinear body-fitted grid. *Comput Fluids* 2020;196:104324. [\[CrossRef\]](#)
- [44] Issakhov A, Zhandaulet Y, Nogaeva A. Numerical simulation of dam break flow for various forms of the obstacle by VOF method. *Int J Multiph Flow* 2018;109:191–206. [\[CrossRef\]](#)
- [45] Li YL, Yu CH. Research on dam-break flow induced front wave impacting a vertical wall based on the CLSVOF and level set methods. *Ocean Eng* 2019;178:442–462. [\[CrossRef\]](#)
- [46] Marsooli R, Wu W. Three-Dimensional numerical modeling of dam-break flows with sediment transport over movable beds. *J Hydraulic Eng* 2015;141:04014066. [\[CrossRef\]](#)
- [47] Bao Y, Chen J, Sun X, Han X, Li Y, Zhang Y, et al. Debris flow prediction and prevention in reservoir area based on finite volume type shallow-water model: a case study of pumped-storage hydroelectric power station site in Yi County, Hebei, China. *Environ Earth Sci* 2019;78:577. [\[CrossRef\]](#)
- [48] Landau LD, Lifshitz EM. *Fluid Mechanics*. (Translated by Sykes JB, Reid WH). 2nd ed. Oxford: Butterworth Heinemann; 1997.
- [49] Issa RI. Solution of the implicitly discretized fluid flow equations by operator splitting. *J Comput Phys* 1986;62:40–65. [\[CrossRef\]](#)
- [50] Oliveria PJ, Issa R. An improved piso algorithm for the computation of buoyancy-driven flows. *Num Heat Transf Fundam* 2011;40:473–493. [\[CrossRef\]](#)
- [51] Klefsman KMT, Fekken G, Veldman AEP, Iwanowski B, Buchner B. A volume-of-fluid based simulation method for wave impact problems. *J Comput Phys* 2005;206:363–393. [\[CrossRef\]](#)
- [52] Marsooli R, Wu W. 3-D finite-volume model of dam-break flow over uneven beds based on VOF method. *Adv Water Res* 2012;70:104–117. [\[CrossRef\]](#)
- [53] Soares-Frazão S, Canelas R, Cao ZX, Cea L, Chaudhry HM, Moran AD. Dam-break flows over mobile beds: experiments and benchmark tests for numerical models. *J Hydraul Res* 2012;50:364–375. [\[CrossRef\]](#)
- [54] Verma DK, Setia B, Arora VK. Experimental study of breaching of an earthen dam using a fuse plug model. *int j eng* 2017;30:479–485. [\[CrossRef\]](#)